

**SILICON AND POROUS SILICON – BASED
EXTENDED GATE FIELD EFFECT
TRANSISTOR FOR pH AND CATIONS SENSOR**

EMAD ADNAN SAID KABAA

UNIVERSITI SAINS MALAYSIA

2018

**SILICON AND POROUS SILICON – BASED
EXTENDED GATE FIELD EFFECT
TRANSISTOR FOR pH AND CATIONS SENSOR**

by

EMAD ADNAN SAID KABAA

**Thesis submitted in fulfilment of the requirements
for the degree of
Master of Sciences**

June 2018

ACKNOWLEDGEMENT

“All praises and thanks to ALLAH”

I would like to express my sincere appreciation and heartfelt thanks to my main supervisor, Dr. Naser Mahmoud Ahmed, whose his expertise, guidance, suggestions, time, comments, and, understanding added considerably to my graduate experience. I wish to appreciate the persistent encouragement and support of my co-supervisor Prof. Dr. Mohamad Suhaimi Bin Jaafar for his guidance, and moral support throughout this project.

I would like also to express my appreciation to the staff in the Nano Optoelectronics Research Laboratory for their co-operation, technical assistance and valuable contribution to my work. The assistance from the staff of the Solid State Physics laboratory is also acknowledged.

To be fair I had to extend my special thanks to Dr. Fayroz A. Sabah and my wonderful friend Dr. Sinan A. Abdulateef for their full support, helping hand, and encouragement to completing this study.

Finally, words may not be sufficient to express acknowledgment to my parents and my sisters and brother, for their support and encouragements.

Emad Kabaa

Penang, Malaysia, November 2017

TABLE OF CONTENTS

ACKNOWLEDGEMENT	ii
TABLE OF CONTENTS	iii
LIST OF TABLES	vii
LIST OF FIGURES	viii
LIST OF SYMBOLS	x
LIST OF ABBREVIATIONS	xiii
ABSTRAK	xiv
ABSTRACT	xvi
CHAPTER 1 : INTRODUCTION	
1.1 Introduction	1
1.2 Problem Statement	4
1.3 Research Objectives	5
1.4 Originality of the Study	5
1.5 Outlines of the thesis	5
CHAPTER 2 : LITERATURE REVIEW AND THEORETICAL BACKGROUND	
2.1 Introduction	7
2.2 pH Theory	7
2.2.1 pH Measurements Methods	8
2.2.2 Effects of Measurements Conditions on pH Sensor Review	9
2.3 Silicon	12

2.3.1	Properties of Si Crystal	13
	2.3.1(a) Structure of Crystal Lattice	13
	2.3.1(b) Properties of Crystal Planes (100) and (111)	13
2.4	Silicon Dioxide	15
	2.4.1 Electrolyte-SiO ₂ -Si System	16
2.5	Porous Silicon	20
	2.5.1 The Factors Affecting the Formation of Porous silicon	20
	2.5.1(a) Dependence of Pore Formation on Crystal Orientation	22
	2.5.2 Mechanism of Porous Silicon Formation	23
	2.5.3 Morphological Characteristics of Porous Silicon	26
	2.5.4 Porous Electrode–Electrolyte Interface	26
	2.5.5 Porous Silicon Biochemical Sensors Review	28
	2.5.5(a) Porous Silicon pH sensor Review	29
2.6	Extended Gate Field Effect Transistor	31
	2.6.1 Nernst Equation	37
	2.6.2 n-MOSFET	38
	2.6.3 Electrolyte Solutions	39
	2.6.4 EGFET Biochemical Sensor Review	40
2.7	Selectivity and Potentiometric Selectivity Coefficient	43
CHAPTER 3 : METHODOLOGY AND CHARACTERIZATION TOOLS		
3.1	Introduction	46
3.2	Preparation of Si Wafers	47
3.3	Anodization System for Porous Silicon Formation	48

3.4	Preparation of Electrolytic Solutions	50
3.5	Structure and Setup of Sensor	51
	3.5.1 Reference Voltage Sensitivity	53
	3.5.2 Drain-Source Sensitivity	53
	3.5.3 Hysteresis Measurements	54
3.6	Selectivity Coefficient Measurements	54
3.7	The Measurements Tools	55
	3.7.1 MOSFET	55
	3.7.2 Source Meters	56
	3.7.3 Reference Electrode	57
3.8	Characterization Equipment	57
	3.8.1 Field Emission Scanning Electron Microscopy (FESEM)	57
	3.8.2 Atomic Force Microscopy	59
	3.8.3 XRD	60
	3.8.4 Hall Effect Measurement System	61
	3.8.5 Optical Reflectometer	63
CHAPTER 4 : RESULTS AND DISCUSSION		
4.1	Introduction	65
4.2	Characteristics of Si (111), Si (100), PSi (111), and PSi (100)	65
	4.2.1 The Electrical Properties	65
	4.2.2 The Surface Morphology	66
	4.2.3 The Crystalline Properties	71
4.3	n-MOSFET Output Characteristics	71
	4.3.1 $I_{DS}-V_{DS}$ Curve for the Saturation Region	71

4.3.2	I_{DS} - V_{GS} Curve for The Linear Region	72
4.4	EGFET Chemical Sensor	73
4.4.1	pH Sensitivity	73
4.1.1(a)	Hysteresis	80
4.4.2	Na^+ , K^+ , Ca^{2+} , Mg^{2+} Sensors	81
4.5	The Potentiometric Selectivity Coefficient	93
CHAPTER 5 : CONCLUSION AND FUTURE WORKS		
5.1	Conclusion Remarks	96
5.2	Future Direction	95
REFERENCES		100
LIST OF PUBLICATIONS		112

LIST OF TABLES

		Page
Table 1.1	An expanded list of some diseases linked to acidity.	2
Table 1.2	Cations concentrations of the human blood plasma.	3
Table 2.1	Summary literature review of Measurements Conditions on pH Sensor	12
Table 2.2	Summary of the factors affecting the formation of porous silicon	23
Table 2.3	The comparison between ISFET and EGFET devices	33
Table 2.4	Summary literature review of EGFET pH sensor	42
Table 2.5	Summary literature review of cations selectivity	45
Table 3.1	The molecular weights of four salts within human blood plasma components	50
Table 3.2	The weights of the dissolved salts in one litter DI for all cations concentrations	51
Table 4.1	Electrical properties of Si (111), Si (100), PSi (111), and PSi (100).	66
Table. 4.2	The pH sensitivities for the four samples Si (111), Si (100), PSi (111), and PSi (100) V_{Ref} and I_{DS} terms	78
Table. 4.3	The pH voltage sensitivity for SiO ₂ /Si for some previous studies	78
Table 4.4	The pH sensitivity for PSi in this study and previous studies	79
Table 4.5	The hysteresis depths in (mV) unit for all devices	80
Table 4.6	The selectivity of Na ⁺ , K ⁺ , Mg ²⁺ , and Ca ²⁺ of some previous studies	92
Table 4.7	Summary of sensitivity and hysteresis results extracted for all samples in this study of the five cations.	93
Table 4.8	The reference voltage values of the four samples for H ⁺ , Na ⁺ , K ⁺ , Mg ²⁺ , and Ca ²⁺ at cations concentration 0.1 M	94
Table 4.9	The calculated potentiometric selectivity coefficient for all samples.	94

LIST OF FIGURES

		Page
Figure 2.1	Silicon unit cell: FCC diamond structure.	13
Figure 2.2	Miller indices of crystal planes for (100) (111).	14
Figure 2.3	SiO ₂ / electrolyte interfacial.	17
Figure 2.4	Electrical double layer (EDL) in SiO ₂ / electrolyte interfacial.	18
Figure 2.5	Explains the effect of crystal orientation on pore shape in: (a) (100) (b) (111).	23
Figure 2.6	The overall chemical reaction to the formation of n-type Psi.	25
Figure 2.7	Equivalent electrical circuit for the reaction between Psi electrode and electrolyte.	28
Figure 2.8	Schematic diagram of (a) MOSFET (b) ISFET (c) electrical equivalent circuit for both, MOSFET and ISFET	31
Figure 2.9	Schematic diagram shows EGFET structure for biochemical sensing applications.	35
Figure 2.10	EGFET <i>I-V</i> characteristics	36
Figure 3.1	The methodology and fabrication process.	47
Figure 3.2	AFM images of n-type PSi with different orientations: (a) (111) (b) (100).	49
Figure 3.3	Schematic diagram of anodization system used for Psi formation	52
Figure 3.4	Schematic diagram of EGFET cations sensor measurement system.	56
Figure 3.5	Schematic diagram of MOSFET (CD4007UBE). (a) A top view of terminal diagram (b) The functional diagram.	57
Figure 3.6	Keithley model 2400 source measurement unit (SMU).	57
Figure 3.7	Ag/AgCl reference electrode from Hanna instruments model HI5311.	58
Figure 3.8	Field-emission Scanning Electron Microscope equipment.	60
Figure 3.9	Atomic Force Microscopy, Bruker Dimension Edge equipment.	61
Figure 3.10	PANalytical X'Pert PRO MRD PW3040 X-Ray diffraction equipment.	62
Figure 3.11	Hall effect system, HL550PC.	62

Figure 3.12	Schematic of Van der pauw technique used in Hall effect system.	63
Figure 3.13	The Optical Reflectometer system, Filmetrics F20.	64
Figure 4.1	AFM images of n-type wafer silicon with different orientations: (a) (111) (b) (100).	67
Figure 4.2	FESEM images of n-type wafer silicon surface with different orientations: (a) (111) (b) (100).	67
Figure 4.3	AFM images of n-type PSi with different orientations: (a) (111) (b) (100).	68
Figure 4.4	FESEM images of PSi layers (a) (100) surface (b) (100) layer cross section (c) (111) surface (d) (111) layer cross section.	69
Figure 4.5	FESEM images of PSi (111) layer cross section explain the pores growth paths.	70
Figure 4.6	XRD patterns with single sharp peak for (a) (111) plane (b) (100) plane.	71
Figure 4.7	Characteristics of MOSFET model CD4007UBE.	72
Figure 4.8	I - V characteristic of EGFET for pH sensor.	75
Figure 4.9	V_{Ref} sensitivity and linearity of EGFET pH sensor (V_{Ref} vs pH).	76
Figure 4.10	I_{DS} Sensitivity and linearity of EGFET pH sensor ($\sqrt{I_{DS}}$ vs pH).	77
Figure 4.11	Hysteresis depths of the four samples in the pH loop 7–4–7–10–7.	81
Figure 4.12	The I - V characterization of EGFET for Na^+ sensors in linear and saturation region.	82
Figure 4.13	The I - V characterization of EGFET for K^+ sensors in linear and saturation region.	83
Figure 4.14	The I - V characterization of EGFET for Ca^{2+} sensors in linear and saturation region.	84
Figure 4.15	The I - V characterization of EGFET for Mg^{2+} sensors in linear and saturation region.	85
Figure 4.16	Sensitivity and linearity of EGFET Na^+ sensor (a) V_{Ref} vs $[\text{Na}^+]$ (b) $\sqrt{I_{DS}}$ vs $[\text{Na}^+]$.	88
Figure 4.17	Sensitivity and linearity of EGFET K^+ sensor (a) V_{Ref} vs $[\text{K}^+]$ (b) $\sqrt{I_{DS}}$ vs $[\text{K}^+]$.	89
Figure 4.18	Sensitivity and linearity of EGFET Ca^{2+} sensor (a) V_{Ref} vs $[\text{Ca}^{2+}]$ (b) $\sqrt{I_{DS}}$ vs $[\text{Ca}^{2+}]$.	90
Figure 4.19	Sensitivity and linearity of EGFET Mg^{2+} sensor (a) V_{Ref} vs $[\text{Mg}^{2+}]$ (b) $\sqrt{I_{DS}}$ vs $[\text{Mg}^{2+}]$.	91

LIST OF SYMBOLS

a_{H^+}	Hydrogen ion activity
a_A	The activities of the dissolved ion A
a_B	The activities of the dissolved ion B
β	Sensitivity parameter
B	Magnetic field
C	Gate capacitance
C_{DL}	Double layer capacitance
Cl_B^-	Chloride ions in bulk solution
e^-	Electron
E	Electrochemical potential
E_0	Electrochemical potential under standard conditions
F	Faraday constant
h^+	hole
H_B^+	Hydrogen ion in the bulk of the electrolyte
hkl	the Miller index
\hbar	Planck constant
I_{DS}	Drain-source current
K	Boltzmann constant
K_a	Acidic constant
K_b	Basic constant
K_+	Cation constant
K_-	Anion constant
$K_{A,B}^{pot}$	Selectivity coefficient
M	Molarity
M_{Wt}	Molecular weight

n	Integer number
N_S	Total number of surface site per unit area
n_s	The sheet carrier density
Na_B^+	Sodium ions in bulk solution
pH_{pzc}	pH at the point of zero charge
q	Electron charge
R	Gas constant
$R_{eq,n}$	Equivalent resistance
T	Absolute temperature
μ_0	Electron mobility
$V_{Chemical}$	Potential of electrochemical cell
V_{DD}	DC voltage that is supplied to the drain of MOSFET
V_{DS}	Drain-source voltage
V_{GS}	Gate-source voltage
V_{Ref}	Reference voltage
V	Volume
V_H	Hall voltage
V_T	Threshold voltage
w	Weight of dissolved
$\frac{W}{L}$	Width-to-length ratio of the MOSFET channel
z_A	The charge numbers of the ion A
z_B	The charge numbers of the ion B
ψ	Surface potential
ν	Frequency
φ_o	Surface potential at electrolyte/insulator interface
χ^{sol}	Surface dipole potential of the solvent

ϕ_M/q	Metal work function
λ_m	Factor modulation of channel length
λ	The wavelength of the X-ray source
θ	The diffraction angle

LIST OF ABBREVIATIONS

AFM	Atomic force microscopy
CMOS	Complementary metal oxide semiconductor
CNT	Carbon nanotube
DC	Direct current
DI	Distilled water
EDL	Electrical double layer
EGFET	Extended Gate Field Effect Transistor
FESEM	Field emission scanning electron microscope
FET	field effect transistors
HBP	Human blood plasma
ISFET	Ion sensitive field effect transistor
IUPAC	The International Union of Pure and Applied Chemistry
<i>I-V</i>	Current-voltage
MOSFET	Metal-oxide-semiconductor field-effect transistor
MSM	Mixed Solution Methods
PEC	photo-electrochemical
PSi	Porous silicon
PSiNWs	Porous silicon nanowires
RCA	Radio Corporation of America
RGOF	Reduced graphene oxide film
RMS	Root-Mean-Square
SiNWs	Silicon nanowires
SOI	Silicon on insulator
SSM	The separate solution method
XRD	X-ray diffraction

TRANSISTOR KESAN MEDAN GET LANJUTAN BERASASKAN SILIKON DAN SILIKON BERLIANG UNTUK PENDERIA PH DAN KATION

ABSTRAK

Berikutan perkembangan sensor biokimia yang berasaskan silikon berliang (PSi) pada penghujung abad ke-20, beberapa kajian telah dijalankan untuk menggunakan kelebihan sifat intrinsik PSi untuk pembangunan sensor biokimia. Silikon (Si) jenis-n komersial telah digunakan dalam dua bentuk, iaitu lapisan permukaan rata dan berliang berasaskan transistor kesan medan get diperluaskan (EGFET), sebagai sensor untuk pH dan kation (Na^+ , K^+ , Mg^{2+} , dan Ca^{2+}). Kajian ini bertujuan memperbaiki kepekaan silikon yang rendah sebagai sensor kation dengan meningkatkan luas permukaan melalui cara yang murah dan mudah. Kajian ini memperoleh pencirian Si dan PSi melalui penggunaan dua orientasi (111 dan 100) dengan memperbaiki dan mencapai kepekaan silikon yang tinggi untuk EGFET berasaskan sensor pH, Na^+ , K^+ , Mg^{2+} dan Ca^{2+} . Selain itu, kajian ini mengkaji kepilihan Si dan PSi terhadap H^+ , Na^+ , K^+ , Mg^{2+} dan Ca^{2+} ; dan fenomena histeresis sebagai petunjuk kestabilan sensor. Ia telah digunakan dalam cara elektromekanikal untuk membentuk struktur berliang bagi kedua-dua orientasi Si (100 dan 111) dengan mempertimbangkan nilai tetap untuk parameter yang mempengaruhi proses punaran kimia. Parameter yang digunakan telah dipilih secara eksperimen (ketumpatan arus, pencahayaan, kepekatan larutan dan suhu). Ciri-ciri morfologi lapisan silikon berliang (PSi) telah dikaji melalui mikroskopi elektron imbasan pancaran medan. Diameter liang untuk PSi (111) berada dalam julat dari 250 nm hingga 750 nm dengan ketebalan lapisan PSi sebanyak 18.94 μm . Dalam pada itu, diameter liang untuk PSi (100) berada dalam julat 1 μm hingga 6 μm dengan ketebalan 55.37 μm . Sistem penderiaan ion berasaskan EGFET telah dibangunkan dan

kepekaan terhadap pH, Na⁺, K⁺, Mg²⁺ dan Ca²⁺ telah dikira menggunakan kepekaan voltan dan arus salir rujukan. Luas permukaan PSi yang tinggi mencapai nilai kepekaan pH yang lebih tinggi berbanding permukaan rata. Kepekaan PSi (100) melebihi nilai Nernst secara teori (59.2 mV/pH) iaitu 72.3 mV/pH, manakala untuk PSi (111) nilainya ialah lebih kurang 56 mV/pH. Dalam pada itu, respons permukaan rata Si (111) lebih baik berbanding Si (100). Fenomenon histeresis merupakan petunjuk kestabilan dan kebolehbalikan dalam respons perlahan pada pH 7, dan kitaran 7-4-7-10-7 diukur untuk setiap sampel. Kedalaman histeresis lebih kecil di bahagian berasid (9, 12, 23 dan 25 mV) berbanding di bahagian asas (9, 17, 63 dan 44 mV) untuk PSi (111), PSi (100), Si (111) dan Si (100) masing-masing. Keputusan di atas disokong oleh kepilahan Na⁺, K⁺, Mg²⁺ and Ca²⁺. Keunggulan PSi juga ditunjukkan dari segi kepilahan natrium [58.4 dan 54.92 mV/pNa untuk PSi(111) dan PSi(100) masing-masing]. Pekali kepilahan potensiometri dikira dengan menggunakan cara larutan berasingan. Keputusan menunjukkan kepilahan tinggi PSi (100) dan Si (111) untuk H⁺, PSi (111) untuk Ca²⁺ serta Si (100) untuk Na⁺. Kesimpulan, kajian ini menunjukkan bahawa luas permukaan ialah faktor penting and utama untuk mempertingkatkan kepekaan membran terhadap ion. Oleh yang demikian, PSi boleh digunakan sebagai elektrod kepilahan ion dalam bidang kimia, biologi dan perubatan kerana ia memperoleh nilai kepilahan yang baik dan melebihi nilai Nernst secara teori di samping kelinearan yang tinggi. Selain itu, kepilahan silikon ion berubah mengikut perubahan orientasi habluran dan morfologi permukaan silikon.

SILICON AND POROUS SILICON – BASED EXTENDED GATE FIELD EFFECT TRANSISTOR FOR pH AND CATIONS SENSOR

ABSTRACT

Following the advances in biochemical sensors based on porous silicon (PSi) in the late 20th century, several studies have been carried out to take advantage of the intrinsic properties of PSi for development of biochemical sensors. The commercial n-type silicon (Si) has been used in two forms, namely, flat surface and porous layer based on extended gate field effect transistor (EGFET), as sensors for the pH and cations (Na^+ , K^+ , Mg^{2+} , and Ca^{2+}). This study aim is to improve the low silicon sensitivity as a cations sensor by increasing the surface area in a cheap and simple way. This study characterizes Si and PSi by using two orientations (111 and 100) in improving and achieve high sensitivity of silicon for pH, Na^+ , K^+ , Mg^{2+} , and Ca^{2+} sensors based EGFET. Also, this study investigates the selectivity of Si and PSi for H^+ , Na^+ , K^+ , Mg^{2+} , and Ca^{2+} ; and hysteresis phenomena as an indicator of sensor stability. It has been used the electrochemical method to form the porous structure for the two Si orientations (100 and 111) considering the fixed values for the parameters affecting the chemical etching process. The used parameters were selected experimentally (current density, illumination, concentration of solution, etching time, and temperature). The morphological characteristics of porous silicon (PSi) layers were investigated by field-emission scanning electron microscopy. The pore diameters for PSi (111) ranged from 250 nm to 750 nm with PSi layer thickness of 18.94 μm . By contrast, the pore diameters for PSi (100) ranged from 1 μm to 6 μm with thickness of 55.37 μm . Ion-sensing system based on EGFET was developed and the sensitivity for pH, Na^+ , K^+ , Mg^{2+} , and Ca^{2+} was calculated using the reference voltage and drain

current sensitivity. The high surface area of P*Si* achieved pH sensitivity values higher than that of the flat surface. The sensitivity of P*Si* (100) exceeded the Nernst theoretical value (59.2 mV/pH), which equal to 72.3 mV/pH, whereas that of P*Si* (111) was approximately 56 mV/pH. By contrast, the response of Si (111) smooth surface was better than that of Si (100). Hysteresis phenomenon was the indicator for stability and reversibility in slow response at pH 7, and cycle 7-4-7-10-7 was measured for each sample. The hysteresis depth was smaller on the acidic side (9, 12, 23, and 25 mV) than that on the basic side (9, 17, 63, and 44 mV) for P*Si* (111), P*Si* (100), Si (111), and Si (100), respectively. The above results were supported by the selectivity of Na⁺, K⁺, Mg²⁺, and Ca²⁺. The superiority of P*Si* was also shown in terms of sodium selectivity [58.4 and 54.92 mV/pNa for P*Si*(111) and P*Si*(100), respectively]. The potentiometric selectivity coefficient was calculated by using separate solution method. Results showed high selectivities of P*Si* (100) and Si (111) for H⁺, P*Si* (111) for Ca²⁺, and Si (100) for Na⁺. It was concluded from this study that surface area is an important and essential factor for increasing the sensitivity of membrane to ions. Therefore, P*Si* can be used as ion selective electrode in the chemical, biological, and medical fields, because it obtains good sensitivity values beyond the theoretical Nernst value with high linearity. In addition, the silicon selectivity of ions changes with the change of the crystalline orientations and the morphology of the silicon surface.

CHAPTER 1

INTRODUCTION

1.1 Introduction

Silicon (Si) is considered the best material of all semiconductors. Nowadays, Si is used in approximately 98% of the structure of electronic devices. Si chips in electronic transplantation devices, including neurostimulators, pacemakers, programmable pumps, and cochlear implants. Si is used because it helps in reducing the size of such devices and provides easy collection, data processing related to the body, and manufacturing precision [1].

Porous Si (PSi) was accidentally discovered by the Uhlirs in 1956. This discovery remained neglected until the 1970s when This discovery remained neglected until the 1970s when a significant level of interest arose with respect to the material, as it was found to be useful as a model of the crystalline Si surface for spectroscopic and chemical sensor applications. In the last decades, researchers have taken a serious interest in PSi-based biochemical sensors. The superior electrical and optical properties make PSi an adaptable material. In addition to its nanomorphological surface (with surface area of up to several hundreds of square meters per one cubic centimetre), its crystalline core properties are different from that of bulk crystalline Si [2]. PSi is a biocompatible material, which means that coating with certain substances to render compatibility is unnecessary. PSi has been used in a wide range of biosensing applications, including sensors for proteins and DNA, bacteria, human serum albumin, and fibrinogen absorption [3].

The acidity (pH) is a major factor influencing biological processes and chemical reactions. pH control improves biochemical reactions and prevents

undesirable interactions. In addition, pH is indicative of the biochemical properties, especially the solubility in solutions and the rate of reaction speed [4].

Diseases are often diagnosed based on unhealthy cells or the growth of bacteria or viruses. However, the real reason for unhealthy cells or bacterial or viral growth is due to a disorder in the acid–base balance. Unhealthy cells appear due to poor nutrition and highly acidic diet. Moreover, cancerous tumors are symptoms to the release of excessive acid wastes. Even the growth of germs and viruses is activated under certain acidic environments. Thus, acidity is the reason for most diseases [Table 1].

Table 1.1: An expanded list of some diseases linked to acidity [5].

Arteriosclerosis	Diabetes	loss of teeth
High cholesterol	Multiple sclerosis	Chronic fatigue syndrome
Cardiovascular disease	Cancer	Dementia
High blood pressure	Immune deficiencies	Depression
Heart attacks	Chronic infections	Premature aging
Stroke	Kidney disease	Arthritis
Hormonal imbalances	Prostate problems	Bone fractures
Insulin insensitivity	Parkinson’s disease	Osteoporosis
Obesity	Candidiasis	Osteoarthritis
Weight problems	Tooth decay	Muscular dystrophy

In human blood, the suitable balance of blood acidity can affect the entire body. A pH change of less than 0.03 units significantly weakens the body’s performance. Many diseases, including arthritis, cancer, and heart disease, are related to acidic or alkaline blood.

In cases of allergies and insomnia, a slight increase in the alkalinity of blood is sufficient to stop the generation of large amounts of acidic products that lead to serious periodic attacks [6]. The destruction of blood cells inside the brain causes Alzheimer’s disease and dementia. These symptoms appear when the acidity of the blood reaches pH 6.6 [7].

A healthy cell has an electromagnetic negative charge and an acidic environment has an electromagnetic positive charge. Thus, the negative charge attracts the positive charge. This phenomenon increases the probability of damage of healthy cells, which leads to the growth of cancerous tumors [8].

Viruses, bacteria, and fungi (including yeast and molds) prefer an acidic environment for growth, proliferation, reproduction, and survival [5]. Various health concerns have increased continuously, forcing many researchers to take seriously ground-breaking studies regarding the effect of pH on human health, particularly cancer.

Human blood plasma (HBP) is a liquid component of blood and presents about 55% of the total blood volume in the human body. HBP contains four cations: Sodium (Na^+), Potassium (K^+), Calcium (Ca^{2+}), and Magnesium (Mg^{2+}). Table 1.2 shows the normal concentration range for the four cations.

Table 1.2: Cations concentrations of the human blood plasma [9].

Cation	The range concentration (mM)
Sodium (Na^+)	142
Potassium (K^+)	5
Calcium (Ca^{2+})	2.5
Magnesium (Mg^{2+})	1.5
pH range	7.25 pH

The essential nutrients obtained from the diet are dietary minerals which are of utmost importance in cells and fluids in the human body.

Sodium ions (Na^+) in the body help control and regulate the level of fluids inside the body. A slight decrease in Na^+ leads to diarrhea and then low body fluid intake, which causes circulatory failure. The opposite enhances water retention, leading to hypertension [10]. Potassium ion (K^+) is one of the major cations inside the cells in the human body. K^+ plays a key role to regulate the level of body fluids, heartbeats, and nerve impulses [11]. The function of calcium ions (Ca^+) in the

construction and maintenance of skeleton and teeth prevents osteoporosis as well as help in blood clotting and transmission of nerve signals and muscle contraction [12]. Several enzymes contain magnesium ions (Mg^{+}). On this basis, Mg^{+} is responsible for freeing energy from food to benefit the body [13]. The imbalance in the four cation concentrations above in the human blood is an important factor in several diseases, including brain injuries, heart disease, high blood pressure, diabetes, neurological diseases, and orthopedic diseases, as well as in pregnancy [14].

1.2 Problem Statement

Ions detections in aqueous solution is very important for environmental and industrial monitoring, bio-agricultural and medical processes, etc. One of the most informative parameter of the electrolyte solutions is the multi-ions selectivity. Exploring new materials with high sensitivity and efficiency for the immobilization and detection of biosignals and conversion of biochemical signal into quantifiable electronic signal is very important importance in biosensor research. Among the variety of proposed concepts and different types of biochemical sensors for ions selection of electrolyte solutions, the integration of chemically or biologically active materials with semiconductor field-effect devices based on an electrolyte-insulator-semiconductor (EIS) system is one of the most attractive approaches. Change of ions concentrations in electrolyte leads to corresponding change of surface potential and thus leads to change of flat-band voltage (i.e. insulator-semiconductor interface depletion layer capacitance) of EIS device. The aim of this study is fabrication multi-ions selective electrode, which has a high sensitivity for multi-ions in same time, which makes the sensors smaller and less expensive using a single electrode to select multiple ions instead of several electrodes.

1.3 Research Objectives

This project investigated the characterizations of silicon and PSi in ions sensors based EGFET. PSi has been utilized to obtain higher sensitivity in ions sensors when compare with Si and other thin films membrane as an extended gate for filed effect transistor.

The main objectives of this project are:

1. To study exploit the morphological properties of n-type PSi of two orientations (111 and 100) in improving and achieve high sensitivity of porous silicon based EGFET for pH, Na⁺, K⁺, Mg²⁺, and Ca²⁺ ions sensors.
2. To investigate hysteresis phenomena as an indicator of sensor stability by slow measurement.
3. To investigate the selectivity of Si (111), Si (100), PSi (111), and PSi (100) for hydrogen, sodium, potassium, magnesium, and calcium ions.

1.4 Originality of the Study

The main originality of this study lies in the characterization of Si and PSi n-type (111)- based EGFET as pH, Na⁺, K⁺, Ca²⁺, and Mg²⁺ sensors via two terms of ion sensitivity, which are reference voltage and drain–source current functions. Furthermore, the potentiometric selectivity coefficient for all above membranes was calculated using the separate solution method (SSM).

1.5 Outlines of the thesis

Generally, the contents of this thesis are orderly as follows:

Chapter 1 presents a brief introduction and the important of pH, Na⁺, K⁺, Ca²⁺, and Mg²⁺ for human body.

Chapter 2 includes a literature review of PSi formation mechanism and describes some applications as biochemical sensor by using Psi, and the SiO₂/electrolyte interfacial theory. This chapter includes also, literature review of EGFET as chemical sensor and the EGFET sensing mechanism.

In Chapter 3, the details on the methodology, general principles underlying the operation of the characterization tools and the experimental details are discussed.

The Si and PSi results obtained with EGFET and their applications are analysed, and discussed **in Chapter 4**.

In Chapter 5, the conclusion and future works are covered.

CHAPTER 2

BACKGROUND AND LITERATURE REVIEW

2.1 Introduction

In this chapter, literature review of the PSi, EGFET, and their bio-chemical applications are presented. Overviews of PSi formation mechanism by photo-electrochemical process, EGFET structure, and theoretical frame of the device which prepared in this study are discussed.

2.2 pH Theory

In 1909, Danish biochemist Lauritz Sorensen suggested the pH symbol as a function of hydrogen ion concentration $[H^+]$. He defined pH as a negative Briggsian logarithm of $[H^+]$, and “power of hydrogen” was abbreviated as “pH” [15]:

$$pH = -\log_{10}[H^+] \quad (2.1)$$

The logarithmic pH scale ranges from 1 to 14. The pH value at 7 is considered the neutral point (the pH of pure water) due to the equal ion concentrations of H_3O^+ and OH^- . The solution becomes acidic as it approaches pH1, whereas pH14 is the strongest base [16].

The International Union of Pure and Applied Chemistry (IUPAC) defines pH as [15]:

$$pH = -\log_{10} a_{H^+}. \quad (2.2)$$

In Equation 2.2, pH is not a function of the total concentration of hydrogen ions in the solution but only for the concentration of active ions (hydrogen ion activity a_{H^+}), which is slightly less than the total concentration [17].

2.2.1 pH Measurements Methods

The measurement of pH is depending on the number of dissociable H^+ in an electrolyte. There are two main methods to determine the pH value: optical and potentiometric methods.

Optical method includes a photometric and visual analyses for the changing of color by the pH effect. The principle of optical method is based on the color changing of specific organic pigments at a specific pH, these organic materials are called color indicators, such as methyl, which color changes in an aqueous solution at a pH of 4.9 from red to yellow. Although this method is quick to determine pH value, but it is inaccurate and gives a rough estimation [18, 19]. By photometric method, pH determination depends on the light source, which is shedding on the target and measuring the absorbance. The measurements via this method are affected by interference, and the equipment has a large size [20]. The area of application for optical pH measurement, be it visual or photometric, is very limited. If the solution to be measured is cloudy or has an inherent color, the measurements will be unreliable. Some measurement solutions also contain chemical bonds which destroy the color indicators through oxidation or reduction and produce incorrect results.

Potentiometric methods use the electrical potential of a sensing electrode as a function to $[H^+]$ according to Nernst equation. An external voltage is applied on the two electrodes (two half-cells) of electrochemical cell under static conditions. At the equilibrium point of electrochemical cell, no current flows through the electrolyte, the ions of solution will align on the electrodes, and each electrode attracts the ions which has opposite charge. By this way, the measurement can be determined along the pH range from 0 to 14, unlike the optical methods [21]. According to the Brønsted–Lowry theory, acids are substances which are capable of separating hydrogen ions. Bases on the other hand enable the deposition of hydrogen ions. A distinction is made between

weak and strong acids and bases. Strong acids and bases are generally almost completely dissociated, weak ones on the other hand are only incompletely dissociated. In addition, a distinction is made between the molar concentration (Molarity) and the equivalent concentration (Normality). The molar concentration means moles per liter and the number of dissociable hydrogen ions is still included in the definition of equivalent concentration, i.e. mol/liter divided by the number of dissociable hydrogen ions. The electrode potential can be determined on the basis of the Nernst equation. The measurement voltage is the difference between two electrode potentials. Whether a reaction can proceed depends on the thermodynamic requirements. The decisive factor is the change in free enthalpy.

In the last two decades of the twentieth century, the development of microelectronic devices has made the sensors extremely small, especially the sensors based field effect transistors (FET). Ion sensitive field effect transistor (ISFET) has made a big move in the small sensors industry, because it is a potentiometric sensor. ISFET is appropriate to a lot of biochemical measurements. The operation of ISFET sensors are based on effect of ions electrical potential on drain-source current via an insulator gate, leads to modify the threshold voltage of ISFET [22].

2.2.2 Effects of Measurements Conditions on pH Sensor Review

Many factors influence the pH measurement such as, temperature, sample's conductivity, sensing area, crystalline orientation, and illumination.

The temperature and illumination influence on the pH sensors performance are important. Where temperature appears as a main factor in Nernst equation. Liao and Chou [23] investigated ruthenium nitride (RuN) as H^+ sensing membrane base EGFET. The pH measurements were carried out along pH range 1-13 under wide

temperature domain. The study reported that pH sensitivity value was increasing with temperature rising from 55.51 mV/pH at 5 °C to 64.04 mV/pH under 55 °C. The study examined the effect of illumination on pH response. The sensor response became slower under illumination than in darkness. Light on and light off effects were studied also; response voltage was shifted with light on and light off. The same effects of the parameters above were investigated by Lue *et al.*, [24]; where they used ITO thin film base EGFET pH sensor. Where the sensitivity value rose from 50.8 mV/pH to 61.5 mV/pH with temperature increasing from 25-40 °C; and the measured sensitivity under lighting decreased. Also, the study examined the effect of membrane conductivity on pH sensitivity. The results revealed that the sensitivity and linearity increased with sheet resistance decreased. While Rayanasukha *et al.*, [25] tested TiN thin films Silicon substrates base EGFET at wide temperature range from room temperature to 450°C. The pH-sensitivity of TiN-EGFET devices with different substrate heating temperature of 25, 250, 350 and 450°C was 46.46, 51.72, 59.82, 56.70 mV/pH respectively. The sensor exhibited higher sensitivity at the highest temperature.

Chien *et al.*, [26] proposed carbon-nanotube thin film as an EGFET pH sensor. The study found that the enhancement of electrical conductivity of sensing sample leads to increasing pH sensitivity and linearity. Where, the sample which has a sheet resistance of 1.5 kΩ/sq gave pH sensitivity of 50.9 mV/pH, while the other sample which has the resistance of 8.94 kΩ/sq gives 35.5 mV/pH.

Chi *et al.*, [27] studied the effect of illumination on SnO₂ thin film as pH sensing extended gate of EGFET. The study reported that the pH sensitivity in dark environment was increased to 58 mV/pH in comparing with the sensor response of 56 mV/pH under constant light. Noh *et al.*, [28] and Chen *et al.*, [29] have been interpreted

the illumination exposure effect on the pH sensing via the following: when a semiconductor is exposed to the lighting, leads to perturb the carrier concentrations and then causes a large threshold voltage shift. This disturbance of the carrier concentration occurs because of electron-hole composition at optical radiation, which in turn reduces the density of H^+ on the surface. The study reported that the sensitivity and good linearity of Si₃N₄-gate ISFET device can be achieved at 50 mV/pH and 0.9995 in dark and poor sensitivity linearity of 28.3 mV/pH and 0.8775 in light.

Batista and Mulato [30] studied the effect of the crystalline orientations on the response of fluorine-doped tin oxide films (FTO) as sensing gate of EGFET for pH sensor. The study reported that a polycrystalline structure has higher pH sensitivity of 50 mV/pH than a crystalline structure. The study attributed this to a polycrystalline structure has higher surface roughness. Distinctive contending sites can arise depending on the crystallite orientation, for dissociative adsorption lattice atoms [31]. Subsequently, the different of substrates with various crystallite orientations and sample structures are considered as the key parameter that caverns pH response, as affirmed by Guerra and Mulato [32]. The (001) orientation displays better sensitivity of 38.1 mV/pH, in light of the fact that the particles are arranged almost parallel to each other.

Guidelli *et al.*, [33] investigated V₂O₅/WO₃ as pH sensor base EGFET . The study reported that a more reliable sensor response can be obtained by elevating the immersing time of a sample in the electrolyte; and it has been found that the current drift is perfectly stable after a waiting time of 5 min. The waiting time is depending on the hydration resistance of the membrane surface; thus, the hydration state can enhance the sample's conductivity. The extracted sensitivity was 68 mV/pH and 1.36 (μA)^{1/2}/pH.

Furthermore, the large sensing area is one of important factor to enhance the pH sensitivity. A comparative study was carried out by Li et al. between ZnO nanowires and ZnO thin film for pH response [34]. The study reported that pH sensitivity of ZnO nanowires was greater than ZnO thin film. It was attributed to a larger effective sensing area for the nanowires. In addition, Maiolo *et al.* fabricated nanoporous ZnO as EGFET pH [35]. The study reported that the good pH sensitivity of 50.1 mV/pH due to the large surface area of porous structure which produces more hydroxyl groups to guarantee high ionic conduction.

Table 2.1: Summary literature review of Measurements Conditions on pH Sensor.

Sensing membrane	pH sensitivity		Factor	Reference
	(mV/pH)	(μA) ^{1/2} /pH		
RuN	55.5		Temperature and illumination	[23]
ITO	50.8		Temperature, illumination, and conductivity	[24]
Tin	46.46		Temperature	[25]
Carbon-nanotube	50.9		Electrical conductivity	[26]
SnO ₂	56		Illumination	[27]
FTO	50	0.9	Crystalline orientation	[30]
V ₂ O ₅ /WO ₃	68	1.36	Hydration	[33]
ZnO NWs	46.25	0.73	Sensing area	[34]
ZnO thin film	37.14	0.54		
ZnO	50.1		Sensing area	[35]

2.3 Silicon

The abundance of silicon in the crust of earth is exceeded only by oxygen. It is widely available in most types of water (e.g., oceans) and can be found in various minerals. One of the most important reasons for using Si is that it is cheap and nontoxic. Thus, Si is used in many fields, including electronic device fabrication and biochemical and medical applications.

2.3.1 Properties of Si Crystal

2.3.1(a) Structure of Crystal Lattice

Crystalline Si has the structure of diamond, which belongs to the cubic system. The unit cell structure of Si crystal is shown in Figure 2.1, with the density of atoms of approximately 5×10^{22} (atoms/cm³). Si atom forms tetrahedral covalent bonding together with neighboring atoms for having four valence electrons [36].

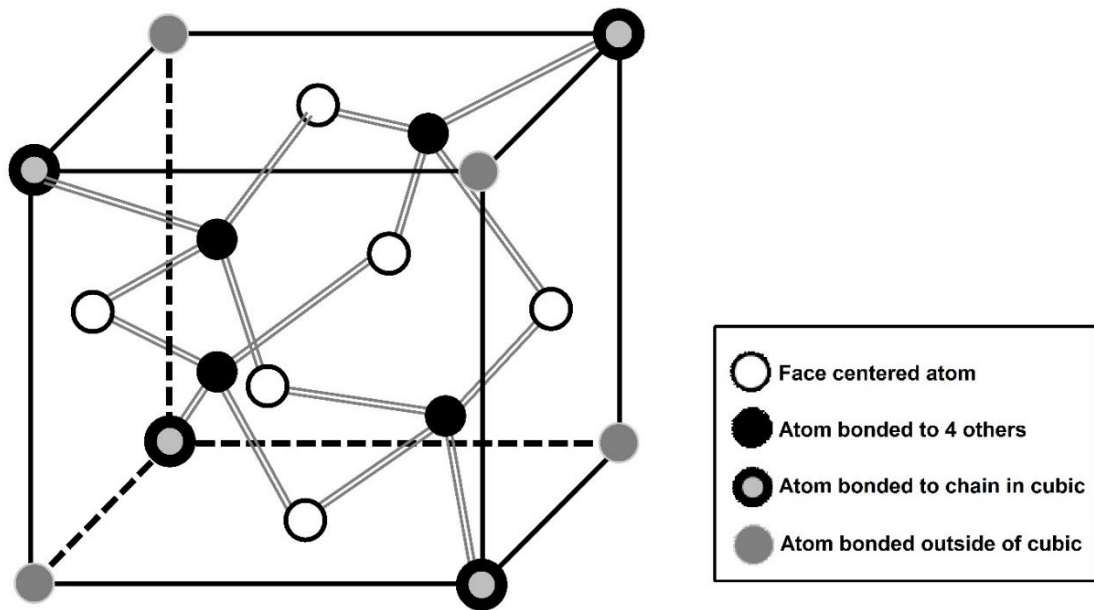


Figure 2.1: Silicon unit cell: Face center cubic (FCC) diamond structure [36].

2.3.1(b) Properties of Crystal Planes (100) and (111)

Crystal orientation responsible for physical, chemical, mechanical, and electronic properties of the crystalline materials. When electronic devices are manufactured on semiconductor substrates, crystallographic planes, particularly the planar arrangement of atoms and the spacing between atomic planes, are considered. Orientation properties depend on the configuration of planar atomic and direction of Si crystal. The penetration of ions into the crystalline lattice varies according to the crystalline orientations primarily because ions channel through open directions.

Figure 2.2 shows the number of atoms in (100) and (111) planes. The atomic planer density of (100) and the available bond density have same value of 6.78×10^{14} atom/cm². Meanwhile, (111) has higher values for the two terms above (up to 15.66×10^{14} and 11.76×10^{14} atom/cm², respectively) [37].

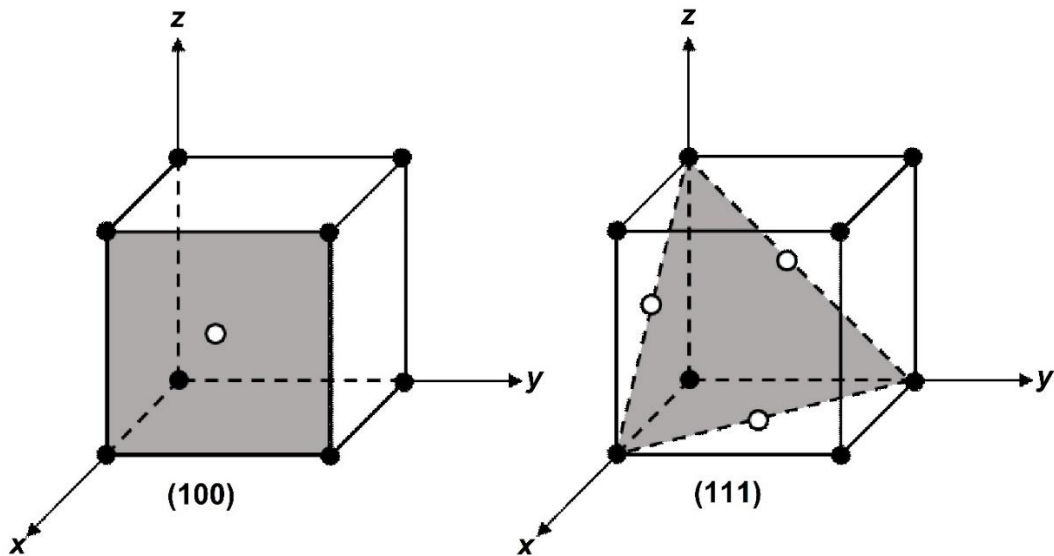


Figure 2.2: Miller indices of crystal planes for (100) (111) [37].

Surface energy is a function of the number of free bonds per unit area of the plane. It is defined in solid physics: the expended work to increase the size of the solid liquid interface, which is a fundamental property of the material that depends on the nature of its bonding with the liquid according to crystal orientations. For the (100) plane, the surface energy is 2.085 J/m^2 , whereas the (111) plane has 1.240 J/m^2 [38].

Mechanically, the (100) plane has the lowest density of atoms. By contrast, (111) plane includes the highest density of atoms. Through experience, it has been found that the (100) wafer chip more easily than (111) wafer with similar shaping processes. It has also generally been noticed that (100) wafers are more difficult to polish to a mirrorlike surface both mechanically and chemically. This may be attributable to less tightly packed atomic structures and faster etch rate of (100) plane

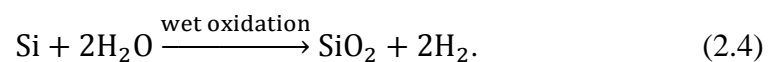
[37]. Depending on the mechanical properties, Si (111) wafers are more appropriate for microelectromechanical systems, torsional micro, and nano-systems [39].

2.4 Silicon Dioxide

Surface preparation is an important aspect for electrochemical measurements, primarily Si. The aim of surface preparation is to earn a clean, homogeneous, and stable surface to obtain repeatable results when re-measuring. The Si on insulator (SOI) consists of Si substrate-covered surface by an insulating layer. One of the most famous types of insulators and the most widely used is Silicon Dioxide (SiO₂). For its electrical properties, SiO₂ emerged as a suitable electronic material for a high degree of device isolation, integrated circuit applications, radiation hardness, devices requiring high speed, and biochemical sensors [40, 41].

Si is always covered by a thin oxide layer, which is generated by Si surface interactions with its chemical environment, including air or aqueous solutions. Si surface tends to react with air to form an oxide layer, which is so-called native oxide. The initial condition for Si electrode properties was taken into account and could be removed by submersion in an HF solution [42].

In the air, the growth rate of native oxide depends on the cleanliness of the air and the initial condition of the surface. The surface of the Si tends to adsorb organic molecules in the air, which in turn reduces the process of forming the oxide layer. In addition, higher concentration of water molecules in the air accelerates native oxide growth. Si chemical reactions with the air are described by the following chemical Equations [43, 44]:



For the initial condition of the surface, native oxide forms on a cleaved surface is faster than the etched surface. The dopant concentration affects the growth rate of the oxide layer, where the heavily doping enhances the oxidation rate. [45]. More available bonds on the surface (or surface bond density) are most widely used to explain the effect of crystal orientation on the oxidation rate. This phenomenon explains that the growth rates of Si(111) are greater than Si(100) because the available bond density for (111) is higher than (100) [46, 47].

2.4.1 Electrolyte / SiO₂ / Si system

For several decades, a mounting attention has occurred in the utilization of insulator semiconductor electrode structure and related devices as sensors. SiO₂ is vastly used in sensor devices for its structural porosity, high permeability to water, easy manufacturing, low cost, and nontoxicity [48].

In the design of an electrolyte-oxide-semiconductor system with a SiO⁺ insulator is of special interest. SiO₂-electrolyte interaction is based on surface adsorption processes, which are in balance with diffusion layer charges. To understand this system, many theoretical studies have been developed to describe its interaction mechanism.

Hydroxyl groups or silanol groups (Si–OH) in the surface of SiO₂ is responsible for an acceptance or donation of the proton from or to the solution, thus providing a positive or negative charge for the surface group. Hydroxyl groups make SiO₂ surface hydrophilic, and it is governing the surface chemistry of Si wafer. Schematically, Figure 2.3 represents the equilibrium that can occur between the Si–OH and solution protons at the SiO₂/solution interface [49].

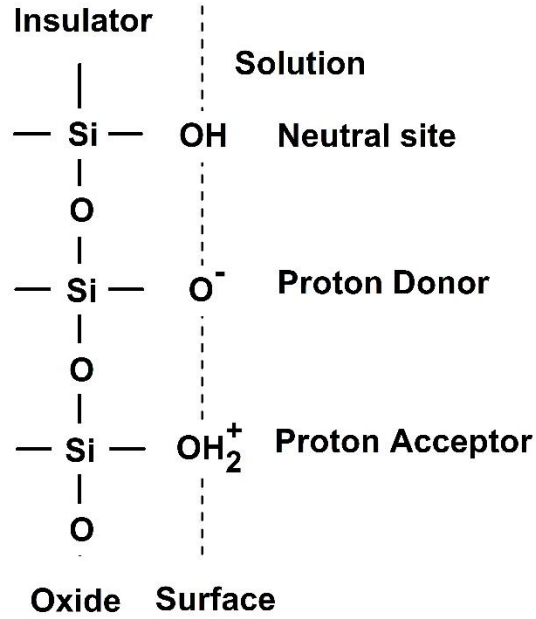
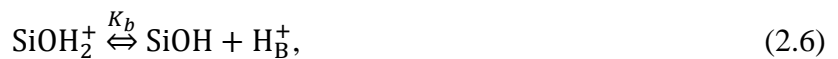


Figure 2.3: SiO₂ / electrolyte interfacial [50].

The site-binding model describes the properties of SiO₂ aqueous electrolyte interface [51]. The equilibrium between the sites of amphoteric SiOH surface and hydrogen ion in the bulk of the electrolyte (H_B^+) can be described by the following Equations [49, 52]:



where K_a and K_b are the amphoteric dissociation (acidic and basic) constants and are given by:

$$K_a = \frac{[SiOH][H^+]_B}{[SiOH_2^+]}, K_b = \frac{[SiO^-][H^+]_B}{[SiOH]}. \quad (2.7)$$

The interactions above explain the reason for naming an amphoteric site, for its capability to bind the protons of solutions neutrally via the acceptance or donation of a proton from the solution to leave a positively or a negatively charged surface group. This phenomenon is similar to the case of pH buffer solutions in which the H⁺ and

OH^- ions are predominant in determining the charge and thus the potential at electrical double layer (EDL). (Figure 2.4).

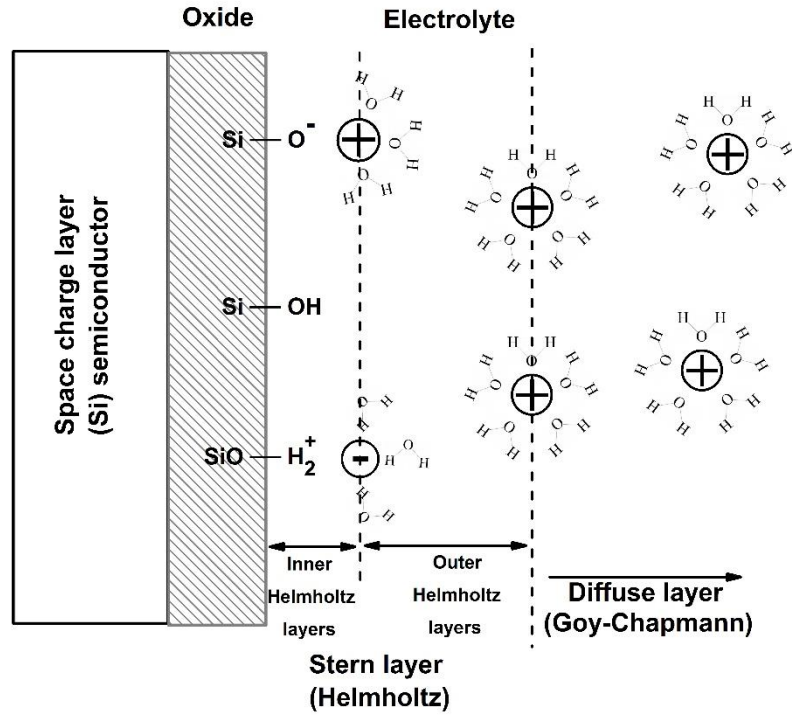
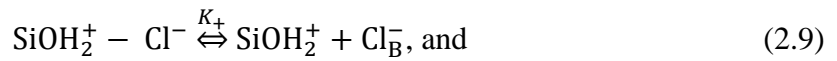
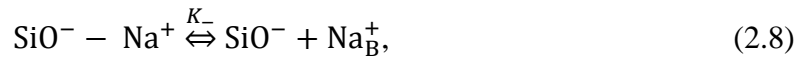


Figure 2.4: Electrical double layer (EDL) in SiO_2 / electrolyte interfacial [53].

The other ions, which support ions in electrolyte, can bind with charged surface sites. This process is named surface complexation. For example, when NaCl solution is used, the equilibrium will be as follows:



$$K_- = \frac{[\text{SiO}^-][\text{Na}^+]_B}{[\text{SiO}^- - \text{Na}^+]}, \quad K_+ = \frac{[\text{SiOH}_2^+][\text{Cl}^-]_B}{[\text{SiOH}_2^+ - \text{Cl}^-]}. \quad (2.10)$$

where: Na_B^+ and Cl_B^- are sodium and chloride ions in bulk solution, K_- and K_+ are the equilibrium constants or dissociation constants for Na^+ and Cl^- .

Surface complexation depends on SiOH_2^+ and SiO^- sites. Surface complexes readjust the equilibrium of acid–base and influence the charge of surface. The total number of surface site per unit area (N_s) is defined by [54]:

$$N_s = [\text{SO}^-] + [\text{SOH}] + [\text{SOH}_2^+] + [\text{SO}^- \text{Na}^+] + [\text{SOH}_2^+ \text{Cl}^-]. \quad (2.11)$$

The surface potential (Ψ) shifted the threshold voltage (V_T) and mainly depends on H^+ concentration in electrolytes, morphological surface, and electrical properties of membranes[55]. In Equation 2.10, surface potential dependence on pH is evident in the individual adsorption of surface sites and surface charge [56]:

$$2.303(\text{pH}_{\text{pzc}} - \text{pH}) = \frac{q\Psi}{KT} + \sinh^{-1} \left(\frac{q\Psi}{\beta KT} \right), \quad (2.12)$$

where q , K , and T denote to the electron charge, the Boltzmann constant, and the absolute temperature, respectively. pH_{pzc} is pH at the point of zero charge (i.e., $[\text{SOH}^+] = [\text{SiO}^-]$), and calculated by [52]:

$$\text{pH}_{\text{pzc}} = -\frac{1}{2} \log(K_+ K_-), \quad (2.13)$$

and β is the sensitivity parameter given by [57]:

$$\beta = \frac{2q^2 N_s \sqrt{\left(\frac{K_a}{K_b}\right)}}{kT C_{DL}}. \quad (2.14)$$

where: C_{DL} presents the double layer capacitance, accordingly to the Gouy–Chapman Stern model.

Equation 2.12 can be rewritten as[58]:

$$\Psi = 2.303 \frac{kT}{q} \frac{\beta}{\beta+1} (\text{pH}_{\text{pzc}} - \text{pH}). \quad (2.15)$$

At SiO_2 -solution interface, ions are distributed parallel to the surface to form the EDL without ion or electron exchange across the borders of their phases.

2.5 Porous Silicon

PSi has an extensive variety of properties that rely upon its microstructure and etching method and permits effectively to increase the selectivity and accuracy of the sensors. In addition, PSi has been widely investigated for many applications, including biochemical sensors [59], drug delivery devices [60], energy storage devices [61], optoelectronics [62], and gas sensors [63].

2.5.1 The Factors Affecting the Formation of Porous silicon

Since the discovery of PSi in the mid-1950s, many methods of forming a porous layer have been developed. Most of these methods are common wet electrochemical etching (easy and cheap). Si can be etched in various electrolytes, including HF and KOH [64].

Several parameters control the electrochemical etching process for Si n-type, including crystalline orientation, dopant concentration, HF concentration, oxidant concentration, current intensity, anodization time, temperature, and illumination.

Najar et al. studied the effect of HF concentration on PSi nanowires (PSiNWs) properties. The study explored that the increasing of HF concentrations generated high lengths and lower diameters for Si nanowires. This finding is due to the increased concentration of HF that increases the dissolution rate of Si. Hence, the rate of dissolution governs electrochemical etching at high electrolyte concentrations [65]. Stapf et al. found that high electrolyte acidity results in rough surface of Si (100) wafer because the speed of etching is low when acidity increases [66].

Three process parameters (dopant concentration, anodization time, and oxidizer concentration) were investigated by Zhong et al. for PSi (100) n-type. Highly doped Si and longer time both contribute to increasing the depth of the pores. The depth of

pores increases with roughness by high H₂O₂ concentration [67]. Cozzi et al. proposed that adding an oxidizer to HF provides more control to pore growth rate via capturing a conduction band electron that is being released during the reaction between fluoride and Si. Consequently, etching rate can be enhanced, and dissolution valence can be reduced [68].

The regularity distribution of dopant concentration in Si wafers plays a vital role for the path of the holes inside the crystalline directions. If the dopant distribution of the Si wafer is irregular, the current flows through low resistance regions (higher doping) faster than lower doping. In other words, etching will be larger in higher doping density regions, causing significant differences between the size of the etched areas and thus allows the surface more nonhomogeneous [69].

Increasing the current density results in expansion of pores, and increasing the current density value, pore diameter, channel shape, pore depth, and roughness allows the surface to obtain disparate pore shape. Hecini et al. [70] and Hasan et al. [71] suggested that increasing HF concentration enhances the current density. Meanwhile, current density is more effective than HF concentration in electrochemical etching.

Kotena et al. investigated the effect of temperature and etching time on surface topography modification of the silicon wafer. Etching rate increases with increasing temperature and prolonged etching time. However, the roughness of surface becomes high due to the high temperature, which increases the etching speed relatively to form uneven surface [72].

Another important parameter in electrochemical etching Si is illumination, especially for n-type low-doped Si. Tsai et al. [73] studied the impacts of illumination during anodic etching of low-doped Si(100) under fixed values of current density and anodization time. The study reported that the density and surface area of pores increase

with increasing illumination intensity. High illumination intensity helps in removing small structures via complete chemical dissolution or oxidation. This phenomenon leads to enhancing the number of Si–O–Si and Si–H groups on the surface of PSi and decreasing the amount of SiH₂ bonds.

2.5.1(a) Dependence of Pore Formation on Crystal Orientation

One striking property of PSi formation is its orientation dependence. This factor is mainly responsible for the shape and size of the pores where the holes are formed in structures following the crystalline orientation. The orientation effect on the etching (dissolution) rate is attributed to the density of surface free bonds. In a more practical meaning, increasing the number of surface free bonds raises the etching rate. This finding is attributed to the etching rate of Si(100) that is faster than (111) because Si(100) has a surface energy higher than (111) given that the surface energy is a function of the number of free bonds per unit area of the plane [68].

Ronnebeck et al. [74] investigated the effectiveness of the crystalline orientation in Si(100) and (111) to form the shape of pores. The study found that the macropore growth direction followed the (100) direction but in (111) orientation. The pores began to grow in the direction of (100) and then diverted to (113) direction. These results agree with the results of this study.

Christophersen et al. [75] studied the morphology of the macropores by using backside illumination. For Si(100), the macropores grew perpendicular on the surface with rough walls, whereas the macropores in Si(111) grew in (111) and (100), and in some cases in (113) directions.

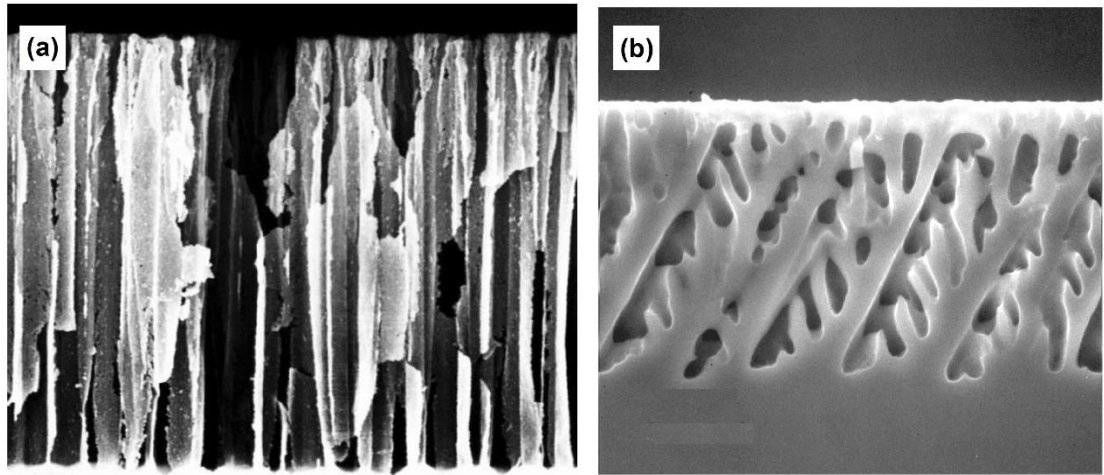


Figure 2.5: The effect of crystal orientation on PSi morphology in : (a) (100) [76] (b) (111) [74].

The growth, shape, and wall roughness of pores based on the crystalline direction of Si are partially understood, and no definitive and specific explanations exist for this phenomenon. We cannot ignore the effect of the other factors on the pore shape. Some studies indicated the effect of other factors, including HF concentration [77], current density [78], and pH value of the electrolytes [79].

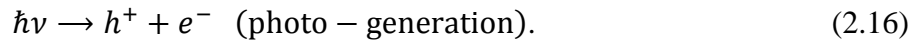
Table 2.2: Summary of the factors affecting the formation of porous silicon.

Porous silicon type	Si type and orientation	Factor	Reference
PSiNWs	n- (100)	HF concentration	[65]
Nano pyramids	p- (100)	HF concentration	[66]
PSiNWs	n- (100)	dopant concentration, anodization time, and oxidizer concentration	[67]
PSi	n- (100)	oxidizer concentration	[68]
PSi	P- (100)	current density	[70]
PSi	P- (100)	current density	[71]
Nano pyramids	p- (100)	temperature and etching time	[72]
PSi	n- (100)	illumination	[73]
PSiNWs	n-(100),(111)	crystalline orientation	[74]
PSi	n-(100),(111)	crystalline orientation	[75]

2.5.2 Mechanism of Porous Silicon Formation

The anodic dissolution Si is controlled by holes, which is supplied at the surface. The major charge carriers for n-type Si are the electrons, and the holes are the minor

carriers. The insufficient holes on the surface in the reverse-biased under anodization lead to a very small etching current. Therefore, the flux of holes is enhanced by illumination, resulting in high current value [80]. Illumination on the surface also contributes to increasing the saturation current in the cathodic region, which is governed by electron diffusion. The discharge of protons caused by the evolution of hydrogen at the Si electrode increases the cathodic current. An n-type Si wafer as an anode is dissolved in HF solution. Given that fluoride ions under illumination energy higher than the bandgap of Si (1.1 eV), the valence band electron adsorbs the energy of photon into the conduction band. This photoexcitation process leaves a hole in the valence band. Subsequently, electron-hole pairs are produced in Si [81]:

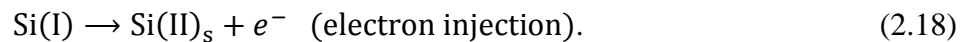


where: \hbar is reduced Planck constant, ν is frequency of absorbed photon, h^+ and e^- are electron-hole pairs

The physical interpretation of the reactions above is that a process of the dissolution at first takes a valence band charge transfer instead of a conduction band charge transfer. When a hole is captured on the surface, the next deficiency is filled by one of the valence electrons in the Si–Si surface bond [81].



The electron incomplete surface bond causes a polarization (i.e., the Si–Si surface bond is minimized on the next site, which in turn generates an effective electric field). Subsequently, an electron from the neighboring site is injected into the Si electrode under the electrical field effect to form Si(II) intermediate.



Losing of covalent electrons in Si(II) intermediate creating the Si–Si bonds of a surface atom is weak and easy to break. Thus, fluorine ions attack these atoms quickly